Joint panel shear yielding in steel moment

Faramarz Rahiminia & Hisashi Namba
Kobe University, Japan

SUMMARY:
This research program was conducted to find a deep understanding in the effects of joint panel shear deformation on elasto-plastic behavior of the beam-to-column connections and to present a new rational design method for the beam-to-column connections. Fourteen full-scale beam-to-column subassemblies were experimentally tested under cyclic loading and results of careful global and detail observations are reported. Main parameters in this investigation were the joint panel strength ratio, weld joint detail, material toughness and width to thickness ratio of column flange. It is shown that cumulative plastic rotation capacity of beam component is almost constant regardless of the amount of joint panel shear deformation and frame total cumulative plastic rotation capacity is increased by increase of joint panel shear deformation.

Keywords: Joint panel, shear deformation, crack initiation, failure mode

1. INTRODUCTION

During the past four decades, enormous investigations have been conducted in Japan to find the role of the joint panel shear deformation in moment resisting frames. First studies were carried out in 1960s (Kato, 1969). As a result of this perseverance, joint panel shear deformation as a potential energy dissipation mechanism has been appreciated in Japan and findings in 1995 Hyogoken-Nambu (Kobe) Earthquake, made no change to this understanding.

Same approach to the joint panel shear deformation was developed in the United States since the first investigations in 1970-1980s (Fielding et al., 1971), (Krawinkler, 1975), (Tsai et al., 1995) until Northridge earthquake. Based on observations and further studies within the SAC project, large joint panel shear deformation was recognized as one of the reasons for the brittle fractures in pre-Northridge moment resisting connections (FEMA 267/267B, 1999), (FEMA 355D, 2000); due to this approach in the US, the post-earthquake joint panel design provisions were modified to prevent excessive joint panel shear deformation (FEMA-350, 2000). However, reviewing the SAC reports shows a large amount of scatter in test data, because of the several different parameters employed in the test programs (FEMA 355D, 2000). Considering this fact, including several other investigations which were conducted after the code modification, in which good performance of weak joint panel specimens has been reported, the question arises that if the role of the joint panel shear deformation has been comprehensively understood (Stojadinovic, 2001), (Engelhardt, 2002), (Lee et al., 2005). Moreover, while in the current seismic provisions in the US, weak joint panel design concept is not permitted (AISC-360, 2010), it is allowed in the Japanese connection design provisions (AIJ-RDCSS, 2006). These different approaches show that despite the common sense of the individual behavior of the weak joint panel, its effects on other beam-to-column connection components are not comprehensively clarified yet.

This research program was conducted to find a deep understanding in effects of joint panel shear deformation on elasto-plastic behavior of the beam-to-column connections and to present a new rational design method for beam-to-column connections. Fourteen full-scale beam-to-column sub-assemblies were experimentally tested under cyclic loading and results of careful global and detail observations are reported. Not only global performance of specimens was studied but also the effects of joint panel shear deformation on failure including crack initiation, progress and final failure was investigated. Main parameters in this study were the joint panel strength ratio, weld joint detail, material toughness and width to thickness ratio of column flange.

2. JOINT PANEL SHEAR STRENGTH

Fig.1, illustrates the Japanese approach to the equilibrium condition for calculation of joint panel shear force (Q). In this Figure d_b and d_c are the effective depth of beam and column, respectively calculated as the distance between two flange thickness centerlines.

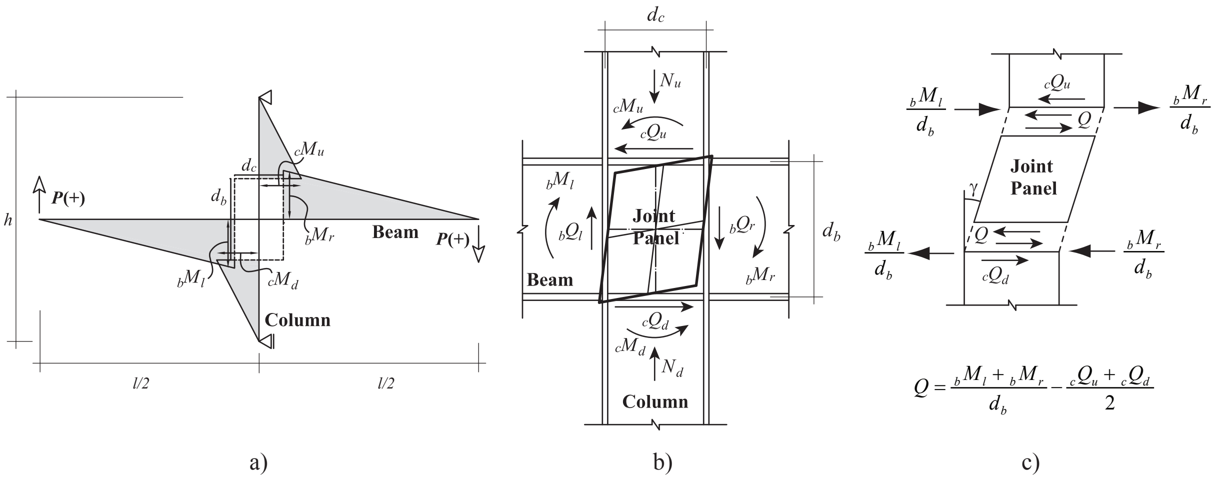

Figure 1. Equilibrium condition of joint panel shear force

According to the Japanese specification, *Recommendation for Design of Connections in Steel Structures* (RDCSS, 2006), the joint panel shear strength Q_p can be calculated as:

$$Q_p = d_c t_w \frac{F_y}{\sqrt{3}} \tag{2.1}$$

Where t_w and F_y are thickness and yield strength of joint panel, respectively. In contrast with the US method for estimation of joint panel shear strength (Eqn.2.2) (AISC-360, 2010), here, the contribution of flexural resistance of column flanges is not considered.

$$R_n = 0.6 F_y d_c t_w \left(1 + \frac{3 b_{cf} t_{cf}^2}{d_b d_c t_w}\right) \tag{2.2}$$

The joint panel to beam strength ratio ${}_{pb}R_p$ is calculated as:

$${}_{pb}R_p = \frac{{}_bM_{pp}}{{}_bM_{bp}} \tag{2.3}$$

Where ${}_bM_{bp}$ is the beam plastic strength and ${}_bM_{pp}$ is the beam moment corresponding to the shear yielding of the joint panel obtained by the following equation and considering the equilibrium condition shown in Fig.1:

$$ {}_{b}M_{pp} = Q_p \cdot d_p \left(\frac{1-\dfrac{d_c}{l}}{a(1-\dfrac{d_c}{l}-\dfrac{d_b}{h})} \right) \qquad \begin{cases} a=1 \ \text{: for exterior column} \\ a=2 \ \text{: for interior column} \end{cases} \tag{2.4} $$

3. EXPERIMENTAL TEST SPECIFICATION AND PROCEDURE

3.1. Test specimens

In this study fourteen full scale specimens were tested as summarized in Table 1. Fig.2 and 3 illustrate the configuration of the specimens, test setup and weld joint details, respectively. Specimens were prepared in two groups of HI as the interior column and HE as the exterior column using two types of weld joint details of field and shop welded joint details. Fillet welds were applied in both sides of the beam web in all specimens.

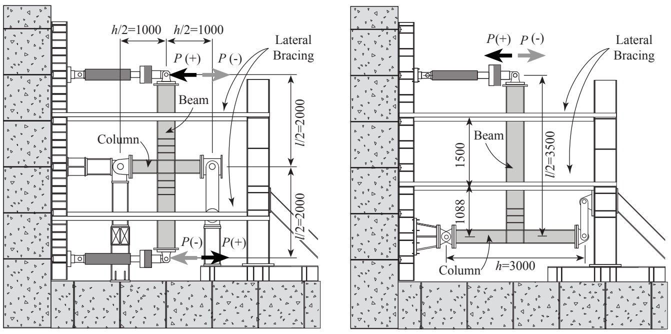

a) HI-series b) HE-series

Figure 2. Test setup

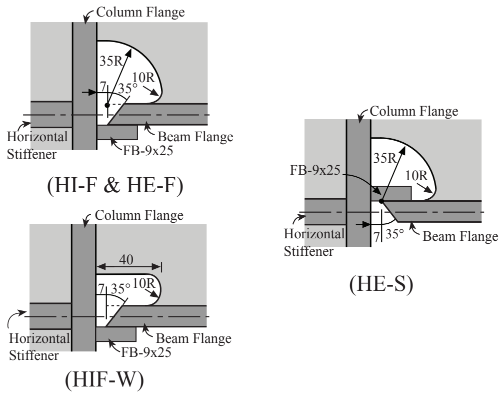

a) Field welded (F-type) b) Shop welded (S-type)

Figure 3. Weld joint details

In this study, one of the main test parameters was the joint panel strength ratio which is provided in Table 1 according to Japanese provisions (${}_{pb}R_p$), in which Q_p is estimated using the coupon test results for column web and doubler plate. To have a wide range of 0.47 to 1.42 for the joint panel strength ratio, specimens were designed with different doubler plate thicknesses. As a reference, two other values of (${}_{pb}U_y$ and ${}_{pb}U_p$) estimated based on the US design provisions (AISC-341, 2010). The ratio of ${}_{pb}U_p$ is calculated using the Eqn. 2.2, and in calculation of ${}_{pb}U_y$ just first term of the equation is used in which the contribution of column flanges is not considered. Another test parameter was the column flange width to thickness ratio (${}_{c}\lambda$). In order to investigate the effect of excessive shear deformation of joint panel on heavy flange column sections, two additional weak panel specimens as HIF-W group with column flange width to thickness ratios of 7 and 5 were prepared which can be considered as a representative of heavy flange column sections commonly used in the US.

3.2. Weld joint details

Fig.3 depicts two types of field and shop welded joint details designed for beam flange to column flange connections using complete joint penetration (CJP) single bevel groove weld with steel backing bar which was left in place. This method is currently the common practice in low to mid-rise steel structural buildings in Japan. In these welds steel run off tabs were used which were left in place to model the most severe practice condition. This method is currently the common practice in low to mid-rise steel structural buildings in Japan. The weld access hole in HI-F, HE-F and HE-S specimens was consisted of two arcs with radiuses of 35 and 10 millimeters. This shape is actually the common post-Kobe earthquake geometry for weld access hole. HIF-W specimens were designed to study the effect of excessive joint panel shear deformation on fracture of beam flange weld joint, so in these specimens, different weld access hole shape was used to ensure that premature beam fracture at weld access hole will not occur.

Table 1. Experimental test specimen specification

Specimens group	Specimen ID	Members	Doubler plate	${}_{pb}R_p$	${}_{pb}U_y$	${}_{pb}U_p$	${}_{cb}R_p$	${}_{c}\lambda$	Weld joint detail
HE-S	HE05S	Beam(SN490B): H-400×200×8×13 Column(SN490B): H-300×300×10×15	-	0.51	0.56	0.65	2.09	10	Shop (S-type)
	HE08S		PL-6	0.81	0.89	0.98			
	HE10S		PL-9	0.96	1.05	1.15			
	HE11S		PL-12	1.09	1.19	1.28			
	HE14S		2×PL-9	1.42	1.55	1.64			
HE-F	HE06F	Beam(SM490A): H-400×200×8×13 Column(SM490A): H-300×300×10×15	-	0.59	0.65	0.76	2.52		Field (F-type)
	HE10F		PL-6	0.96	1.05	1.16			
	HE13F		PL-12	1.26	1.38	1.49			
HI-F	HI06F		PL-9	0.60	0.65	0.71	1.32		
	HI08F		PL-16	0.80	0.87	0.93			
	HI10F		PL-9&12	0.97	1.06	1.11			
	HI13F		2×PL-16	1.27	1.39	1.44			
HIF-W	HI05F-W7	Beam(SM490A): H-400×200×12×19 Column(SM490A): H-300×300×16×22	PL-12	0.48	0.54	0.61	1.10	7	
	HI05F-W5	Beam(SM490A): H-400×200×12×19 Column(SM490A): H-300×300×16×28		0.47	0.54	0.65	1.41	5	

3.3. Material properties

The material utilized for the specimens were hot rolled sections with steel grade SM490A (JIS G 3106) for HI-F and HE-F and SN490B (JIS G 3136) for HE-S specimens. Beam and column sections used for HIF-W specimens were fabricated from plates with steel grade of SM490A (JIS G 3106). Actual material properties obtained by tensile coupon tests are reported in Table 2. One of the other parameter in this study was material toughness. Fig. 4 plots the values of material Charpy impact test results obtained from coupon tests associated with the 'k' area (the meeting point between the web and the flange) of beam and column sections as shown in Fig 4(a).

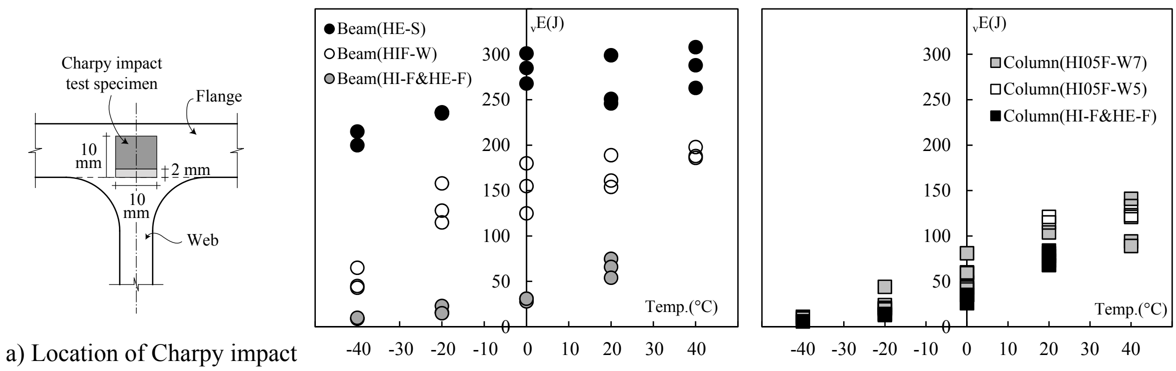

a) Location of Charpy impact test specimen at "K" area

b) Beam material

c) Column material

Figure 4. Charpy impact test results

In Fig. 4(b), beam in HE-S specimens with steel grade of SN490B with an average of 285J at 0ºC have the highest Charpy impact absorbed energy. This value was 153J for HIF-W and beam in HI-F and HE-F specimens have the lowest toughness properties of 33J at 0ºC.

Table 2. Material properties, a) HE-S group

Specimen		Steel Grade	t (mm)	σ_y (N/mm^2)	σ_u (N/mm^2)	YR= σ_y/σ_u	ε_u (%)	EL
Beam	Flange	SN490B	13.0	420	569	0.74	0.17	0.42
	Web		7.90	452	579	0.78	0.19	0.35
Column	Flange		15.2	354	540	0.66	0.18	0.43
	Web		9.83	388	552	0.70	0.19	0.38
Doubler Plate	PL-6		5.73	382	551	0.69	0.26	0.37
	PL-9		9.03	384	550	0.70	0.28	0.39
	PL-12		12.6	366	526	0.70	0.25	0.42
Weld		YGW-11	-	384	506	0.76	0.29	0.36

b) HI-F and HE-F groups

Specimen		Steel Grade	t (mm)	σ_y (N/mm^2)	σ_u (N/mm^2)	YR= σ_y/σ_u	ε_u (%)	EL
Beam	Flange	SM490A	13.0	366	554	0.66	0.22	0.39
	Web		7.91	417	572	0.73	0.21	0.34
Column	Flange		14.7	381	566	0.67	0.21	0.43
	Web		10.0	398	571	0.70	0.21	0.35
Doubler Plate	PL-6		5.88	416	571	0.73	0.21	0.30
	PL-9		8.58	376	541	0.70	0.22	0.37
	PL-12		12.3	377	537	0.70	0.21	0.43
	PL-16		16.2	364	533	0.68	0.23	0.45
Weld		YGW-11	-	459	578	0.79	0.24	0.34

c) HIF-W group

Specimen		Steel Grade	t (mm)	σ_y (N/mm^2)	σ_u (N/mm^2)	YR= σ_y/σ_u	ε_u (%)	EL
Beam	Flange	SM490A	19.1	463	546	0.85	0.24	0.48
	Web		11.8	381	547	0.70	-	0.40
Column	HI05F-W7 Flange		27.7	377	553	0.68	-	0.48
	HI05F-W5 Flange		21.8	377	553	0.68	-	0.48
	Web		15.6	358	535	0.67	0.26	0.44
Doubler Plate	PL-12		11.8	381	547	0.70	-	0.40
Weld		YGW-11	-	504	612	0.82	0.12	0.53

4. TEST RESULTS

4.1. M-θ_t Hysteresis diagrams

M-θ_t hysteresis graphs are shown in Fig.5. In these graphs M and θ_t are beam moment at column face and total rotation, respectively. The graphs in Figs.6 and 7 show the typical cyclic behavior of beam and panel components. All weak panel specimens show a stable M-θ_t hysteresis graph with good estimation of joint panel strength ($_bM_{pp}$) and in balanced and strong panel specimens beam strength ($_bM_{bp}$) shows good correspondence.

4.2. Global view on observation results

4.2.1. Observation method and procedures

During the loading tests, visual inspection was done in each loading cycle of 0.02, 0.04 and 0.06 rad total deformations to observe the crack initiation and progress. Based on pilot studies, five points were determined to be highly potential for cracking. Fig. 8 illustrates the location of these hot spots in each type of weld joint details.

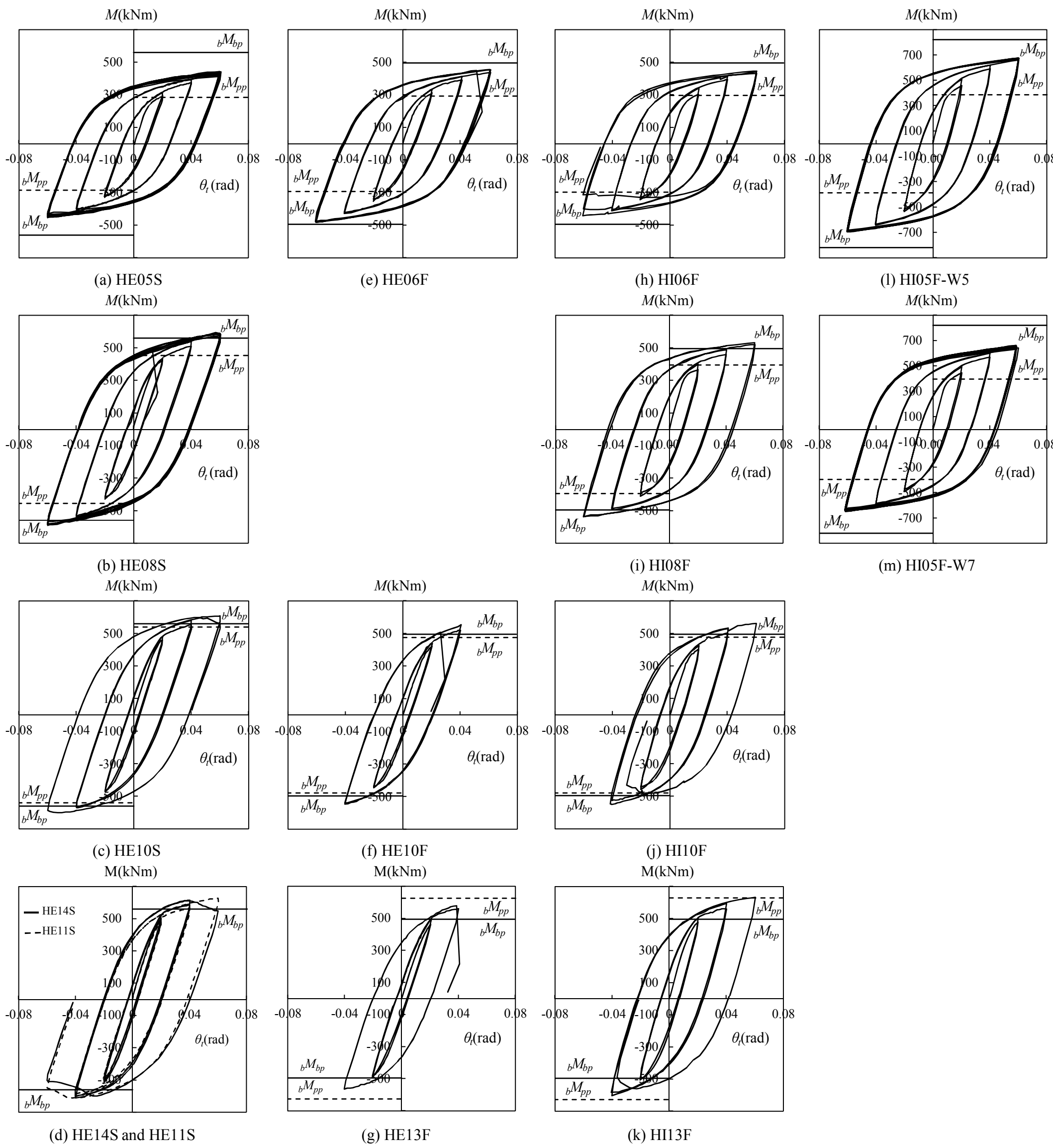

Figure 5. M-θ_t Hysteresis diagrams

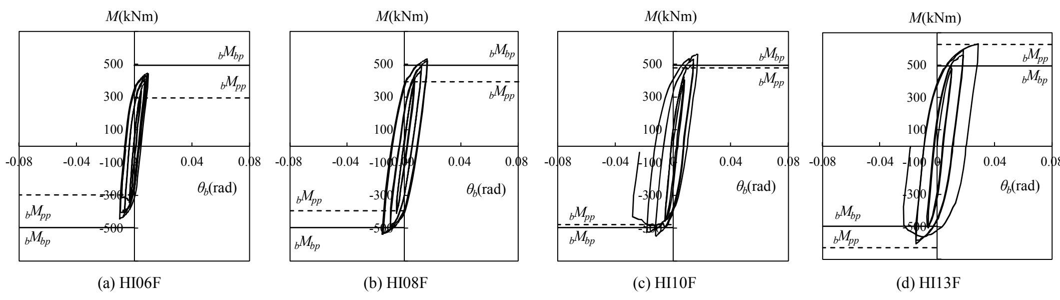

Figure 6. M-θ_b Hysteresis diagrams in HIF specimens

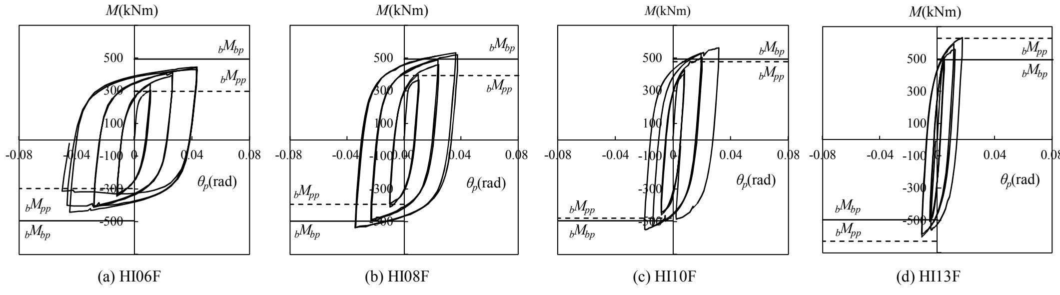

Figure 7. M-θ_p Hysteresis diagrams in HIF specimens

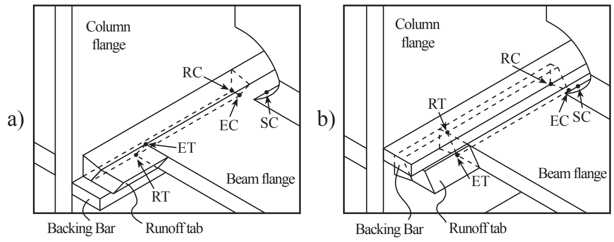

Figure 8. Location of hot spots. a) F-type, b) S-type

4.2.2. Final fracture mode

In this experimental test, typical final failure modes were beam fracture with ductile or brittle patterns and also beam local buckling as shown in Fig.9. In S-type specimens no stiffener was applied to avoid beam local buckling so balanced and strong panel specimens (HE10S, HE11S and HE14S) failed by local buckling as can be seen as a gradual reduction of strength In hysteresis graphs shown in Fig.5(c and d). In all weak panel specimens beam fracture occurred after significant rotation capacity and large joint panel shear deformation with a stable hysteresis behavior as can be seen in the corresponding hysteresis diagrams shown in Fig.5. Among these specimens, just HI06F showed slightly different behavior. During the loading cycles of 0.06 rad, it failed because of a later observed lack of fusion in doubler plate perimeter weld.

The beam fracture pattern was strongly affected by material toughness properties and ambient test temperature as reported in Table 3. Observation of crack surfaces in HE06F, HE10F, HE13F and HI08F specimens, revealed a very small area of ductile crack growth near the tip of the weld access hole, followed by brittle crack through the entire section of the beam flange as illustrated in Fig.10(a). These specimens had low toughness material, which were tested at low ambient temperature (4-16 ºC).
HI10F and HI13F specimens were also fabricated from low toughness material but they were tested at high ambient temperature of 20-30 ºC. In these specimens, a crack pattern with combination of brittle and ductile crack as illustrated in Fig.10(b) was observed. It was started by ductile crack growth from tip

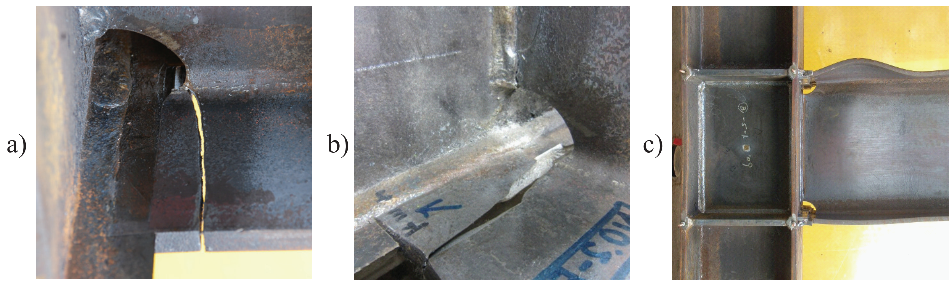

Figure 9. Typical final failure modes. a) Brittle beam fracture from weld access hole, b) Ductile beam fracture from weld access hole, c) Beam local buckling

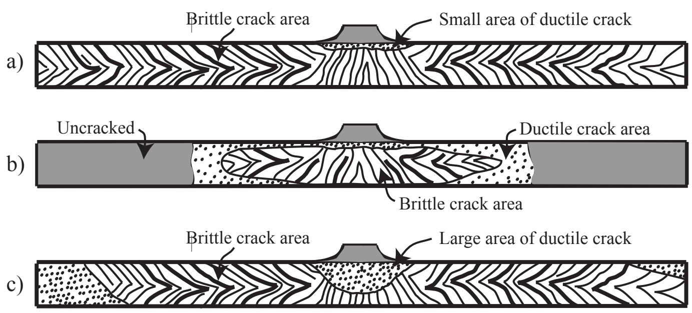

Figure 10. Typical fracture surfaces. a) Brittle crack pattern , b) Combination of brittle and ductile crack pattern, c) Large area of ductile crack pattern

of the weld access hole, followed by a stopped brittle crack progression and again ductile crack progress. HE08S specimen with high toughness material which was tested at 15 ºC, showed a ductile crack pattern consisted of large area of ductile crack started from tip of the weld access hole and edge of slit at runoff tab as illustrated in Fig.10(c).

4.3. Rotation capacity

4.3.1. Beam behavior

In Fig.6 hysteresis diagrams of beam component (M-θ_b) for HIF specimens are presented. It can be observed that while the number of cycles is increased by reduction of joint panel strength ratio, the amount of beam deformation in each cycle of loading is decreased. As a result of this cyclic behavior, near same cumulative rotation capacity for beam component is obtained for all specimens which can be seen in Fig.11(a). As the graph shows the joint panel strength ratio has no detrimental effect on beam component cumulative rotation capacity. The rotation capacities of beam component in HES and HIFW specimens are higher than other specimens due to the superior material toughness as shown in Fig.4.

4.3.2. Joint panel behavior

In Fig.7 hysteresis diagrams of joint panel component (M-θ_p) for HIF specimens are plotted. It can be seen that joint panel shows less deformation in balanced and strong panel specimens compared to weak panel specimens. Furthermore, strong and balanced panel specimens sustained less number of loading cycles, therefore, these specimens showed less cumulative deformation capacity of joint panel component compared to weak panel specimens which can be seen in Fig.11(b). Joint panel components of weak panel specimens in Fig.7 show a stable cyclic behavior with high deformation capacity.

4.3.3. Total deformation

Cumulative total deformation verses joint panel strength ratio is plotted in Fig.11(c). Total rotation capacity is increased by reduction in joint panel strength ratio. We can also find that within weak panel specimens higher total rotation capacity is shown by HIFW and HES specimens due to the higher material toughness properties although the total rotation capacity obtained by weak panel specimens with low toughness material (SM-series) is still satisfactory for seismic applications. In this graph, HIF specimens are shown with hollow circles. In Fig.11(d), the ratios of joint panel deformation to the total deformation for all specimens with different joint panel strength ratios are plotted. The joint panel contribution is increased by reduction in joint panel strength ratio and joint panel and beam components show equal contribution to the total deformation in the balanced condition which is in good agreement with design assumptions.

Table 3. Test results, * JP: Joint panel shear deformation, SB: Brittle fracture from scallop (weld access hole), SD: Ductile fracture from scallop, [SD]: Ductile crack with rapid progress, LB: Beam Local buckling

Specimen	Failure cycle (θ_t)	Failure mode*	$\Sigma\theta_{tpi}$ (rad)	$\Sigma\theta_{bpi}$ (rad)	$\Sigma\theta_{ppi}$ (rad)	η_t	η_b	η_p	$M_{max} / {}_bM_{bp}$	Ambient Temp. (°C)
HI06F	0.06(-3)	JP + [SD]	0.70	0.08	0.61	79.4	10.7	294	0.90	20
HI08F	0.06(+3)	JP + SB	0.65	0.12	0.48	58.9	16.9	237	1.08	16
HI10F	0.06(-1)	SD	0.29	0.09	0.18	22.7	12.7	89.5	1.14	30
HI13F	0.06(-1)	SD	0.32	0.15	0.11	25.3	21.0	54.5	1.28	23
HE06F	0.06(+4)	JP + SB	0.80	0.11	0.70	72.5	9.10	290	0.92	9
HE10F	0.06(+1)	SB	0.21	0.10	0.11	12.6	8.20	46.0	1.12	4
HE13F	0.04(+2)	SB	0.13	0.10	0.03	7.70	8.50	11.9	1.17	8
HE05S	0.06(+13)	JP + SD	2.34	0.29	2.07	217	21.6	878	0.78	15
HE08S	0.06(-7)	JP + SD	1.29	0.49	0.81	81.7	36.4	348	1.05	
HE10S	0.06(-2)	LB	0.47	0.30	0.18	25.5	22.1	75.4	1.08	
HE11S	0.06(-1)	LB	0.30	0.22	0.08	16.4	16.7	35.8	1.12	
HE14S	0.06(-1)	LB	0.31	0.30	0.01	17.0	22.4	3.90	1.10	
HI05F-W7	0.06(+10)	JP + SD	1.94	0.32	1.59	232	38.9	801	0.81	17
HI05F-W5	0.06(-6)	JP +SD	1.31	0.23	1.07	162	27.4	536	0.82	16

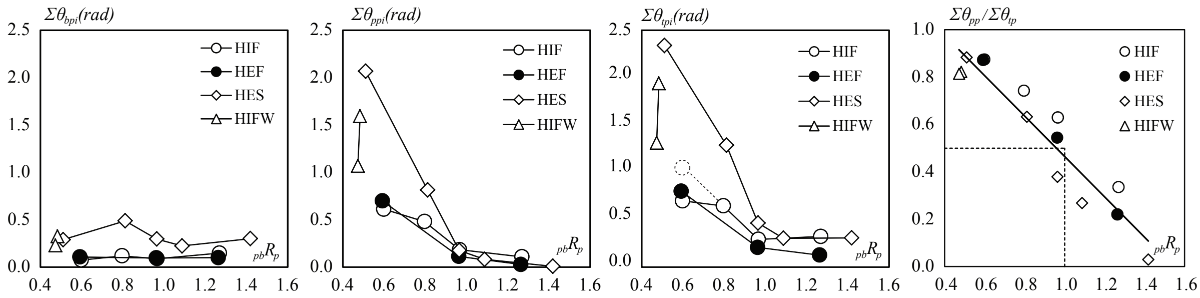

a) Beam component b) Joint panel component c) Total deformation d) Contribution of beam and joint panel

Figure 11. Contribution of each component in cumulative plastic rotation

5. EFFECT OF JOINT PANEL DEFORMATION ON FAILURE

5.1. Crack initiation and progress at tip of the weld access hole (SC)

Fig. 12 shows that in which loading cycle first crack initiation was observed. Crack initiation was defined when 0.2 mm crack opening was observed using crack scale. First crack initiation occurred at earlier stage of loading in strong and balanced panel specimens, shown with solid bars in the Figure, compared to weak panel specimens shown by hollow bars. Crack progress was investigated by plotting the measured crack opening (δ_{co}) verses beam rotation as shown in Fig. 13. In this Figure, η_b is the normalized beam cumulative plastic rotation $\Sigma(\theta_{bpi})$ to beam plastic rotation (θ_{bp}). This parameter was considered as a good index to neglect the effect of difference in beam length in HI and HE specimens. In all specimens, regardless of the joint panel strength ratio, the crack progress was proportional to the beam component deformation. This result that joint panel strength ratio has no effect on crack progress is same as what was shown in Fig.11(a) in which near same cumulative rotation capacity for beam component was observed, regardless of the joint panel strength ratio. The measured final crack opening before failure ($_u\delta_{co}$) is shown in Fig.14. HE05S and HE08S specimens could sustain higher crack opening due to superior material toughness properties so these specimens could show higher beam cumulative plastic rotation as shown in Fig.11(a). Near same final crack opening was observed for HIF and HEF specimens regardless of the joint panel strength ratio but it resulted ductile or brittle fractures due to the ambient test temperature as discussed in 4.1.2.

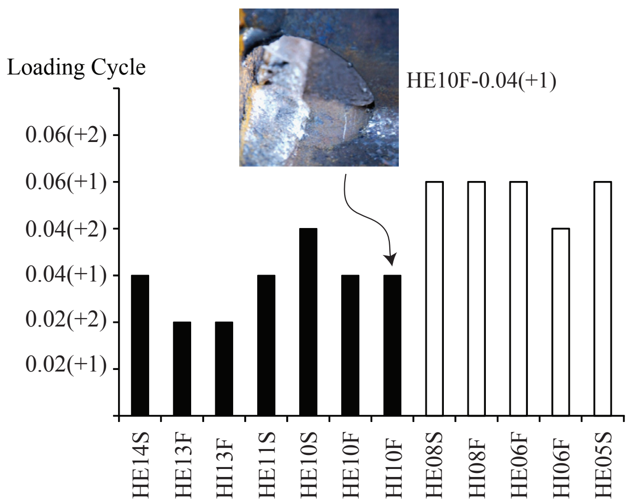

Figure 12. First crack initiation during the loading test

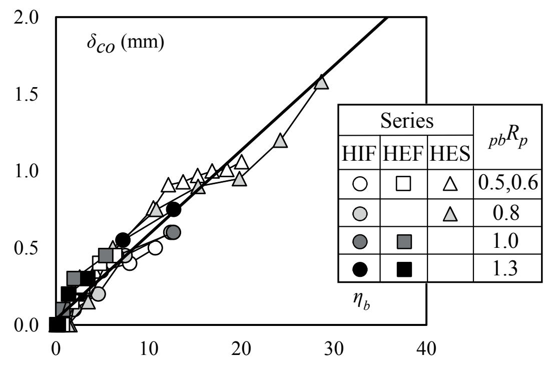

Figure 13. Crack growth (δ_{co}-η_b)

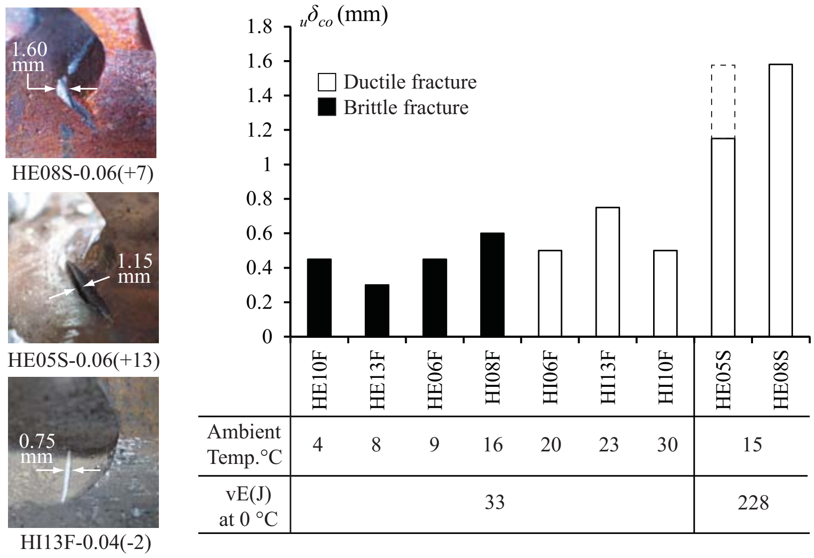

Figure 14. Final crack opening from tip of the weld access hole

6. CONCLUSIONS

In all specimens regardless of joint panel strength ratio and weld joint detail, first crack initiation was observed at tip of the weld access hole. This occurred at earlier stage with higher progress for strong and balanced panel specimens compared to weak panels. The common failure pattern was crack progress from this hot spot. Specimens with higher material toughness could sustain higher crack opening before final failure and in specimens with low material toughness, the failure pattern of ductile or brittle was strongly affected by ambient test temperature. Total rotation capacity was increased by reduction in joint panel strength ratio and higher total rotation capacity was shown by specimens with higher material toughness properties although the total rotation capacity obtained by weak panel specimens with low toughness material was still satisfactory for seismic applications.

ACKNOWLEDGEMENT
The research described in this paper was supported by grants from Ministry of Education of Japan under the project No: 21560591, which is truly acknowledged.

REFERENCES

Kato, B. (1969). Design criteria of joint panel in moment resisting frames subjected to lateral loading, *JSSC Journal of Constructional Steel* **5:50**, 40-44 (in Japanese).
Fielding, D.J. and Huang, J.S. (1971). Shear in steel beam-to-column connections. *Welding Journal* **50:7**,313-s–326-s.
Krawinkler, H., Bertero, V.V. and Popov, E.P. (1975). Shear behavior of steel frame joints. *Journal of the Structural Division* **101:11**,2317–2336.
Stojadinovic, B., Goel, S.C., Lee, K., Margarian, A.G. and Choi, J. (2000). Parametric tests on unreinforced steel moment connections. *Journal of Structural Engineering, ASCE* **126:1**,40–49.
Lee, D., Cotton, S.C., Hajjar, J.F., Dexter, R.J. and Ye, Y. (2005). Cyclic behavior of steel moment-resisting connections reinforced by alternative column stiffener details, II. Panel zone behavior and doubler plate detailing. *Engineering Journal* **14qtr05**,215-238.
Federal Emergency Management Agency (2000). State of the art report on connection performance, Report No. FEMA 355D.
AISC Committee on Specifications, (2010), ANSI/AISC 341-10, Seismic provisions for Structural Steel Buildings.
AIJ Architectural Institute of Japan (2006), Recommendation for Design of Connections in Steel Structures.